Holzem, KM.; Gómez García, JF.; Glukhov, AV.; Madden, EJ.; Koppel, AC.; Ewald, GA.; Trenor Gomis, BA.... (2016). Reduced response to IKr blockade and altered hERG1a/1b stoichiometryin human heart failure. Journal of Molecular and Cellular Cardiology. 96:82-92. doi:10.1016/j.yjmcc.2015.06.008.

Diminished Response to I_{Kr} Blockade and Altered hERG1a/1b Stoichiometry in Human Heart Failure

Katherine M. Holzem, M.S.[1], Juan F. Gomez[2], Alexey V. Glukhov, Ph.D.[1], Eli J. Madden[1], Aaron C. Koppel[1], Gregory Ewald, M.D.[1], Beatriz Trenor, Ph.D.[2], Igor R. Efimov, Ph.D.[1,3]

Affiliations:

[1]Department of Biomedical Engineering, Washington University in St. Louis, MO 63130, USA.

[2]Polytechnic University of Valencia, Valencia, Spain

[3]Moscow Institute of Physics and Technology, Dolgoprudny, Moscow Region, Russia

Corresponding author:

Igor R. Efimov

Department of Biomedical Engineering

Washington University in Saint Louis

390E Whitaker Hall

One Brookings Drive

St. Louis, Missouri 63130-4899

Tel: 1-314-935-8612; Fax: 1-314-935-8377;

E-mail: igor@wustl.edu

Abstract

Rationale: Heart failure (HF) claims 250,000 lives per year in the US, and nearly half of these deaths are sudden and presumably due to ventricular tachyarrhythmias. QT interval and action potential (AP) prolongation is a hallmark proarrhythmic change in the failing myocardium, which potentially results from alterations in repolarizing potassium currents. Thus, we aimed to examine whether decreased expression of the rapid delayed rectifier potassium current, I_{Kr}, contributes to repolarization abnormalities in human HF. To map functional I_{Kr} expression across the left ventricle (LV), we optically imaged coronary-perfused LV free wall from donor and end-stage failing human hearts. The LV wedge preparation was used to examine transmural AP durations at 80% repolarization (APD80), and treatment with the I_{Kr}-blocking drug, E-4031, was used to interrogate functional expression. We assessed the percent change in APD80 post-I_{Kr} blockade relative to baseline APD80 (ΔAPD80) and found that ΔAPD80s are reduced in failing versus donor hearts in each transmural region, with 0.35-, 0.43-, and 0.41-fold reductions in endo-, mid-, and epicardium, respectively (p=0.008, 0.037, and 0.022). We then assessed hERG1 isoform gene and protein expression levels using qPCR and Western blot. While we did not observe differences in *hERG1a* or *hERG1b* gene expression between donor and failing hearts, we found reductions in hERG1a mature protein and a shift in the hERG1a:hERG1b isoform stoichiometry. Computer simulations were then conducted to assess I_{Kr} block under E-4031 influence in failing and nonfailing conditions. Our results confirmed the experimental observations and E-4031-induced relative APD80 prolongation was greater in normal conditions than in failing conditions, provided that the cellular model of HF included a significant downregulation of I_{Kr}.

Conclusions: In human HF, the response to I_{Kr} blockade is diminished, suggesting decreased functional I_{Kr} expression This reduced functional response is associated with altered hERG1a:hERG1b protein stoichiometry in the failing human LV, and failing cardiomyoctye simulations support experimental findings. Thus, I_{Kr} protein and functional expression may be important determinants of repolarization remodeling in the failing human LV.

Key Words: Heart failure, arrhythmias, potassium channels, remodeling, repolarization

Abbreviations

AP=Action Potential; APD=Action Potential Duration; APD80=Action Potential Duration at 80% Repolarization; D=Donor; Endo=Endocardium; Epi=Epicardium; HF=Heart Failure; F=Failing; LV=Left Ventricle; Mid=Midmyocardium.

Introduction

Heart failure (HF) is the end stage of many cardiovascular diseases, in which the heart can no longer support the metabolic demands of the body. HF is an increasing problem in the US, with an estimated 5 million Americans currently afflicted by the disease. Approximately ¼ million HF-related deaths occur annually,[1] nearly half of which are due to sudden cardiac death. These sudden cardiac events are presumably the result of ventricular tachyarrhythmias, which are a consequence of adverse electrophysiologic remodeling during the HF progression.

Action potential (AP) prolongation and resulting QT prolongation are hallmark arrhythmogenic changes in the failing myocardium.[2-5] While increased late sodium current has been demonstrated in association with AP prolongation in HF,[6-8] voltage-dependent potassium currents are critical determinants of cardiac AP duration (APD). In humans, the rapid component of the delayed rectifier potassium current (I_{Kr}) is largely responsible for ventricular repolarization. Tetramers of the hERG1 protein α-subunit, encoded by the *KCNH2* gene, form the channel underlying cardiac I_{Kr}. Two different splice variants of *KCNH2*, both *hERG1a* and *hERG1b*, are expressed in human ventricular tissue, with the *hERG1a* isoform predominating.[9] In various animal models of HF, delayed rectifier potassium currents are reduced. However, in human isolated cardiomyocytes, I_{Kr} amplitude is small, making differences between donor and failing hearts undetectable.[2]

We hypothesized that I_{Kr} is downregulated in human HF, promoting AP prolongation in failing myocardial tissue. Thus, we aimed to investigate functional I_{Kr} expression in the failing human left ventricle (LV) and examine the relative expression of hERG1a and hERG1b isoforms at the gene and protein expression levels. We then conducted cellular and fiber simulation studies to provide further evidence for I_{Kr} downregulation in HF. The regulation of functional I_{Kr} in human HF has not been previously reported; thus, these studies may help elucidate the underpinnings of arrhythmogenic AP prolongation in the failing human heart.

Materials and Methods

Human heart recovery. All studies using human heart tissue have been approved by the Institutional Review Board at Washington University in St. Louis. In total for this study, we recovered 16 donor human hearts, rejected for transplantation from the Mid America Transplant Services (St. Louis, MO), and 14 end-stage failing hearts from transplant recipients at Barnes-Jewish Hospital. All hearts were obtained immediately after removal from the chest in the operating room. Hearts were arrested using ice-cold cardioplegic solution and transported to the laboratory for dissection and functional experiments. Prior to experiments, LV tissue was collected and preserved in RNA later (Sigma-Aldrich, St. Louis, MO) for mRNA or flash-frozen in liquid nitrogen for protein expression analyses.

Optical imaging. Human LV wedge preparations were used for electrophysiologic experiments, as described previously.[3] Briefly, wedges were dissected from an LV marginal branch and were mounted with the transmural surface facing the optical apparatus (Figure 1A-B). Preparations were perfused with oxygenated Tyrode's solution maintained at 37°C, with a perfusion pressure of 60-80 mmHg. Blebbistatin (10-20 μM) was used to immobilize myocardial tissue, and Di-4-ANEPPS was used to map transmembrane potential. Pseudo-ECGs were recorded with Ag/AgCl electrodes placed on either side of the transmural surface, and human intracellular APDs were validated using fixed 3.0 M KCl filled microelectrodes. Tissue was paced using a steady state S1S1 restitution protocol, starting at a pacing cycle length (CL) of 2,000 ms and progressively decreasing to the functional refractory period. Data were analyzed using custom-written MATLAB software.[10] Table 1 shows donor and patient characteristics of hearts used in functional experiments.

Pharmacologic interrogation of I_{Kr}. Following the collection of baseline restitution measurements, we added 1 μM E-4031, a high-affinity I_{Kr} blocker, to the Tyrode's solution. Recordings were collected at 5-minute intervals after drug treatment, until a steady-state AP morphology was achieved (approximately 15-20 minutes). The steady state restitution protocol was then repeated (Figure 1C). Because E-4031 blockade of I_{Kr} is essentially irreversible, we did not conduct drug washout.

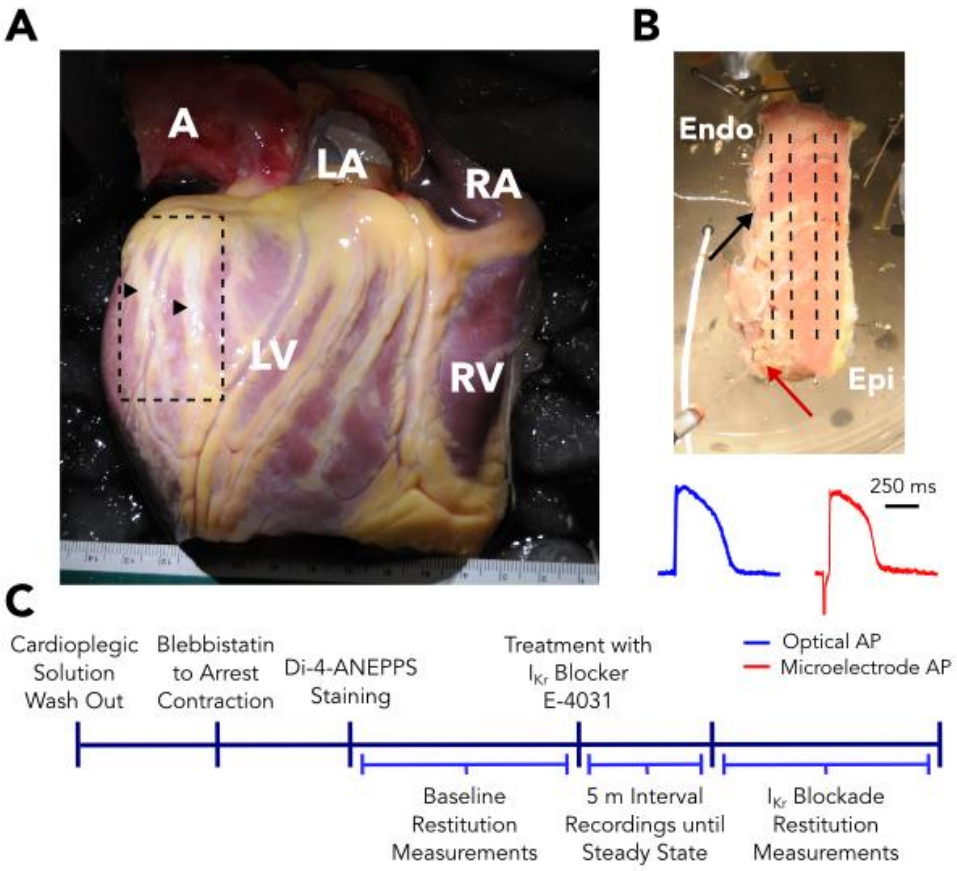

RNA isolation and real-time qPCR. Total RNA was extracted from human LV tissue samples using the RNEasy Fibrous Tissue Mini Kit (Qiagen, Valencia, CA), and RNA yield was quantified and purity assessed using the Nandrop 1000 (Thermo Scientific), as previously described.[11] Total RNA (1-2 ug) was converted to cDNA using the High Capacity cDNA Reverse Transcription Kit (Applied Biosystems, Foster City, CA). Real-time PCR of cDNA was performed with the TaqMan PCR Master Mix on a StepOnePlus sequence detector (Applied Biosystems, Foster City, CA). The *RPL32* TaqMan Gene Expression Assay Hs00851655_g1 was used as an endogenous control, because it is one of the most stable reference genes for cardiac gene expression studies.[12] The TaqMan Gene Expression Assay Hs00165120_m1 was used to detect *hERG1a* mRNA, and custom-made assays were used for the detection of *hERG1b*, as previously described.[12] Data were analyzed using the threshold cycle (Ct) relative quantification method.[11, 13]

Protein expression. Western blot analysis was performed on LV protein lysates, as previously described.[3, 4] Fresh endocardial and epicardial tissues were frozen in liquid nitrogen, pulverized, and

homogenized in super RIPA buffer. Protein was quantified using the BCA Assay (Bio-Rad, Hercules, CA), and equal protein masses were loaded for each sample. SDS-PAGE was carried out using standard methods, and membranes were probed with anti-Kv11.1 antibodies (Alomone, Israel, Jerusalem; Enzo Life Sciences, Farmingdale, NY). Images were acquired with the LAS-4000 mini (Fujifilm, Tokyo, Japan) and analyzed with Multi Gauge software (Fujifilm, Tokyo, Japan). Protein band densities were normalized to GAPDH.

Statistical analysis. Statistical significance was determined by Student's t-test or Welch's t-test. Both one- and two-tailed t-tests were used as appropriate, depending on the whether our experimental prediction indicated a unidirectional change or that the alteration may have occurred in either direction. Paired t-tests were used to compare the same hearts before and after drug treatment, and unpaired tests were used to analyze donor and failing heart groups. The Welch's t-test was selected when a statistically significant p value from f-test ($p < 0.05$) indicated unequal variance between groups.

Human ventricular cell AP modeling. Simulations of endocardial and epicardial cell electrophysiological activity were carried out using one of the most up-to-date human ventricular myocyte models developed by Grandi et al.[14] (GPB model), which was characterized by a thorough description of intracellular calcium handling. Both cellular and one-dimensional strand simulations were performed, and we computed APD at 80% repolarization (APD80). A steady state S1S1 restitution protocol was simulated, starting at a pacing cycle length (CL) of 2,000 ms and decreasing to the functional refractory period. Computational methods are detailed in the Supplementary Materials.

Homogeneous electrophysiological remodeling in HF. To simulate the electrical activity of human failing ventricular myocytes, the GPB model was modified as in Trenor et al.[15] Ionic parameters were changed to describe the hallmark characteristics of failing cardiac tissues and cells, such as AP prolongation and alterations of calcium handling, on the basis of experimental data (see Table 2 for details). To model downregulation of I_{Kr}, we gradually decreased this current up to 90% in different simulations.

Heterogeneous electrophysiological remodeling in HF. Experimental studies describing transmural ion channel expression changes are insufficient from the failing human heart, and most of these studies have been limited to mRNA or protein level investigation.[11, 16-18] Furthermore, extrapolating gene or

protein expression to channel functional activity is not trivial. Thus, on the basis of the limited literature, we included a heterogeneous model of HF based on Gomez et al., where certain parameters were selectively altered in epicardial and endocardial cells.[19] Specifically, the activity of the Na^+/Ca^{2+} exchanger (I_{NCX}), which shows a significant upregulation in failing myocytes, was increased 2-fold in epicardial cells and 1.6-fold in endocardial cells.[18, 20-22] As reported in our experiments, I_{Kr} was also decreased heterogeneously in endocardium (50% reduction) and epicardium (60% reduction) in strand simulations.

Results

APD Restitution with I_{Kr} blockade. To examine transmural effects of I_{Kr} expression in the human LV, we measured optical APs before and after treatment with E-4031. We then analyzed APD80 for each transmural region and constructed APD80 restitution curves by plotting the APD80 duration against the pacing cycle length (PCL) for donor and failing hearts. Baseline APD80 restitution curves for donor hearts (Figure 2A) reveal greater transmural dispersion of APD80s and shorter APs compared with failing hearts (Figure 2B). The longer APs in the failing heart are more pronounced at lower pacing frequencies, leading to steeper restitution curves. In contrast, following E-4031 treatment, APD80s for failing hearts (Figure 2E) are shorter than those for donor hearts (Figure 2D) at each pacing cycle length and restitution curves for failing hearts appear flattened (Figure 2B). APD80 gradients were then calculated at several PCLs by subtracting $APD80_{Endo}$-$APD80_{Epi}$. Transmural dispersion of APD80s was observed for donor hearts without and with E-4031, but not for failing hearts under either condition (Figure 2C,F). In addition, the donor heart APD80 gradients demonstrated a linear relationship with PCL ($R^2 = 0.92$, $p = 0.003$ for baseline; $R^2 = 0.78$, $p = 0.02$ for E-4031), while no relationship was observed between failing heart APD80 gradients and PCL (Figure 2C,F).

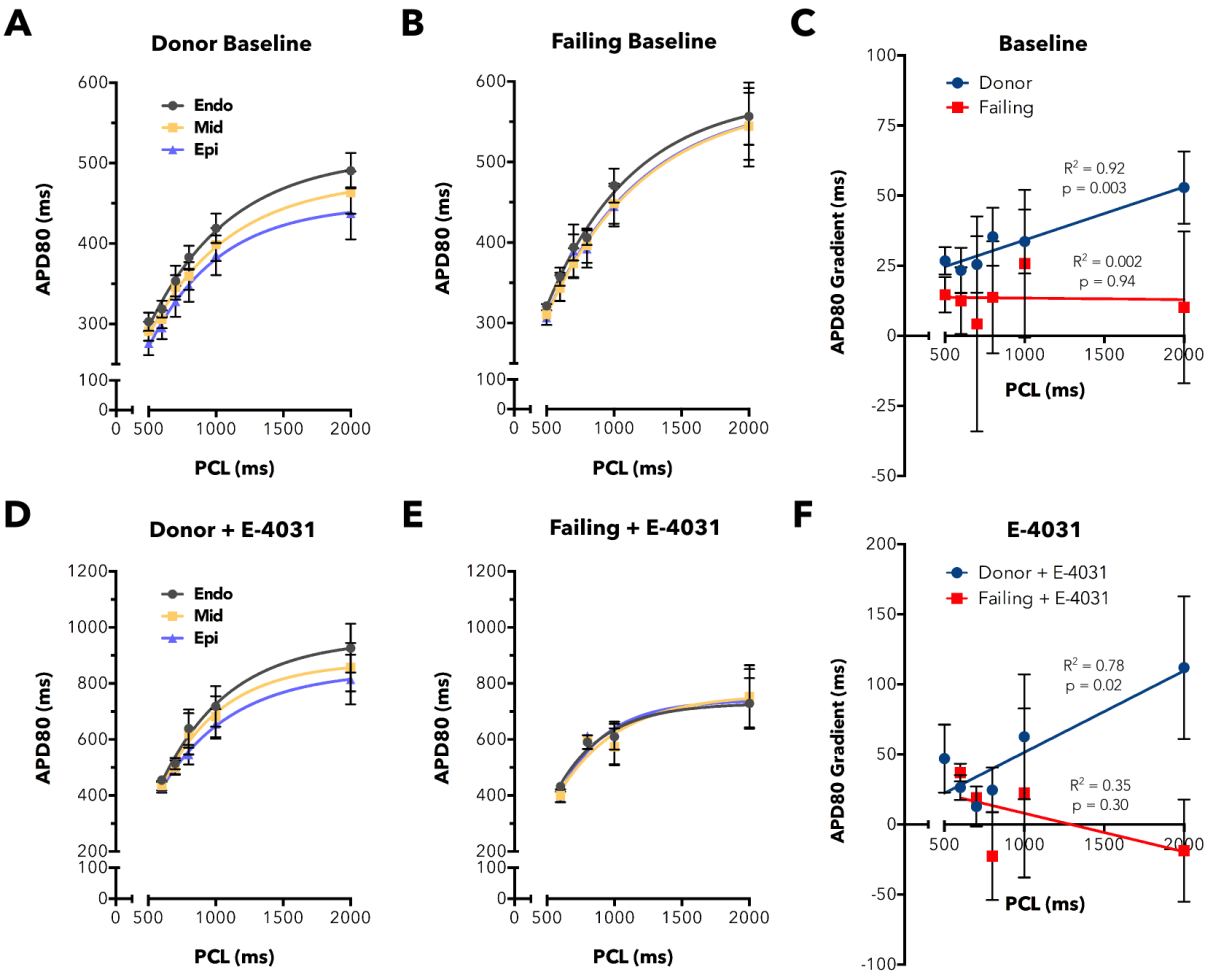

Functional I_{Kr} expression. To assess functional, cell-surface expression of I_{Kr}, we examined APD80 prolongation following E-4031 treatment. Figure 3A,B shows APD80 maps for representative donor and failing human hearts, respectively, at 1000 ms PCL. Corresponding pseudo-ECG recordings and optical recording traces are shown below each map. APD80 maps for the donor heart show the normal APD gradient from endo- to epicardium, and significant prolongation of the APD in each transmural region with I_{Kr} blockade. Conversely, the transmural distribution of APD80 are more uniform in the failing heart under control conditions, consistent with our previous reports.[3, 23] However, the effect of I_{Kr} blockade on transmural APD80s appears reduced.

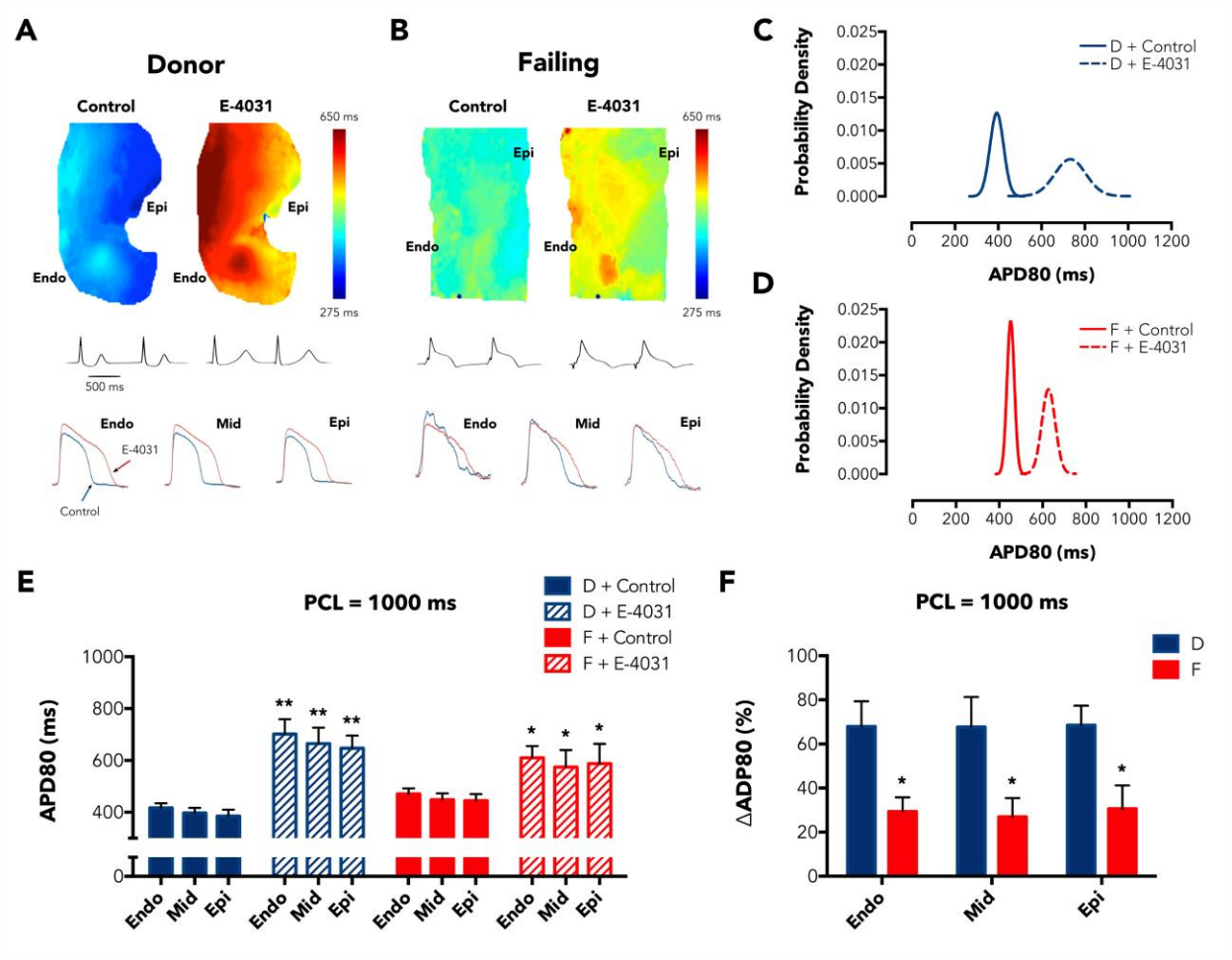

The distribution of APD80s is varied between donor and failing hearts without and with I_{Kr} blockade. Figure 3C,D show APD80 Gaussian distribution curves computed from the means and pooled standard deviations for donor and failing hearts. The distribution curves demonstrate greater separation between the pre- and post-E-4031 conditions for donor hearts compared with failing hearts. This widening between curves is due to the higher baseline APD80s in failing hearts, but even more so from increased APD80s in donor hearts following I_{Kr} blockade. Figure 3E shows average APD80 values for donor and failing hearts under control conditions and with E-4031 treatment (PCLs = 1,000 ms). I_{Kr} blockade in donor hearts results in strongly significant ($p < 0.01$) increases in APD80 in each transmural region; however, while I_{Kr} blockade still leads to transmurally increased APD80s for failing hearts, the differences are less significant ($p < 0.05$). In addition, we calculated the % change in APD80 after E-4031 treatment relative to the control condition, or ΔAPD80 = $[(APD80_{E\text{-}4031}\text{-}APD80_{Control})/APD80_{Control}]*100$, which are greater in the donor hearts for each transmural region. ΔAPD80 values for failing versus donor hearts demonstrate 0.43-, 0.40-, and 0.45-fold reductions in endo-, mid-, and epicardium, respectively

(p=0.020, p=0.033, p=0.013, Figure 3F). Results obtained at the 2,000 ms PCL were consistent with the 1 Hz data and are displayed in Figure S1.

KCNH2 Gene Expression. To examine whether transcriptional regulation of *hERG1a* and *hERG1b* splice variants is responsible for the reduced effect of E-4031 in failing hearts, we analyzed the mRNA expression of both variants in human LV tissue samples. Figure 4A,B show relative quantification values of *hERG1a* and *hERG1b* in donor and failing LV samples. We found no statistically significant differences in the mRNA expression levels when comparing failing to donor human heart tissue ($p = 0.84$ and $p = 0.36$, respectively). Although, *hERG1b* appears reduced in F, the variance for *hERG1b* donor gene expression is large. The majority of the apparent difference in *hERG1b* expression was due to a single sample, which was not excluded by Grubb's analysis. These results suggest that decreased functional I_{Kr} in HF is not due to altered *KCNH2* gene expression or splicing.

hERG1 Protein Expression. Given that post-translational protein processing regulates functional ion channel expression, we then investigated whether altered hERG1 protein expression was associated with functional I_{Kr} downregulation. To do this, we examined hERG1a and hERG1b protein expression levels in endo- and epicardial LV samples. We observed that normalized hERG1a mature protein had a 0.55-fold reduction ($p = 0.51$) in the epicardium of failing compared with donor hearts (Figure 4D), and total hERG1a protein trended toward reduction (Figure 4C). In addition, the stoichiometry of the hERG1a:hERG1b isoforms was altered in failing versus donor hearts, with 0.52- and 0.58-fold reductions in the endocardium and epicardium, respectively ($p = 0.012$ and $p = 0.019$, Figure 4G). Interestingly, hERG1b did not appear altered in failing hearts (Figure 4E,F); however, there was a trend toward increased expression of the immature hERG1b isoform in failing hearts (Supplementary Figure S3). hERG1b data were confirmed by experiments with an alternative antibody and are shown in the supplementary data (Figure S4).

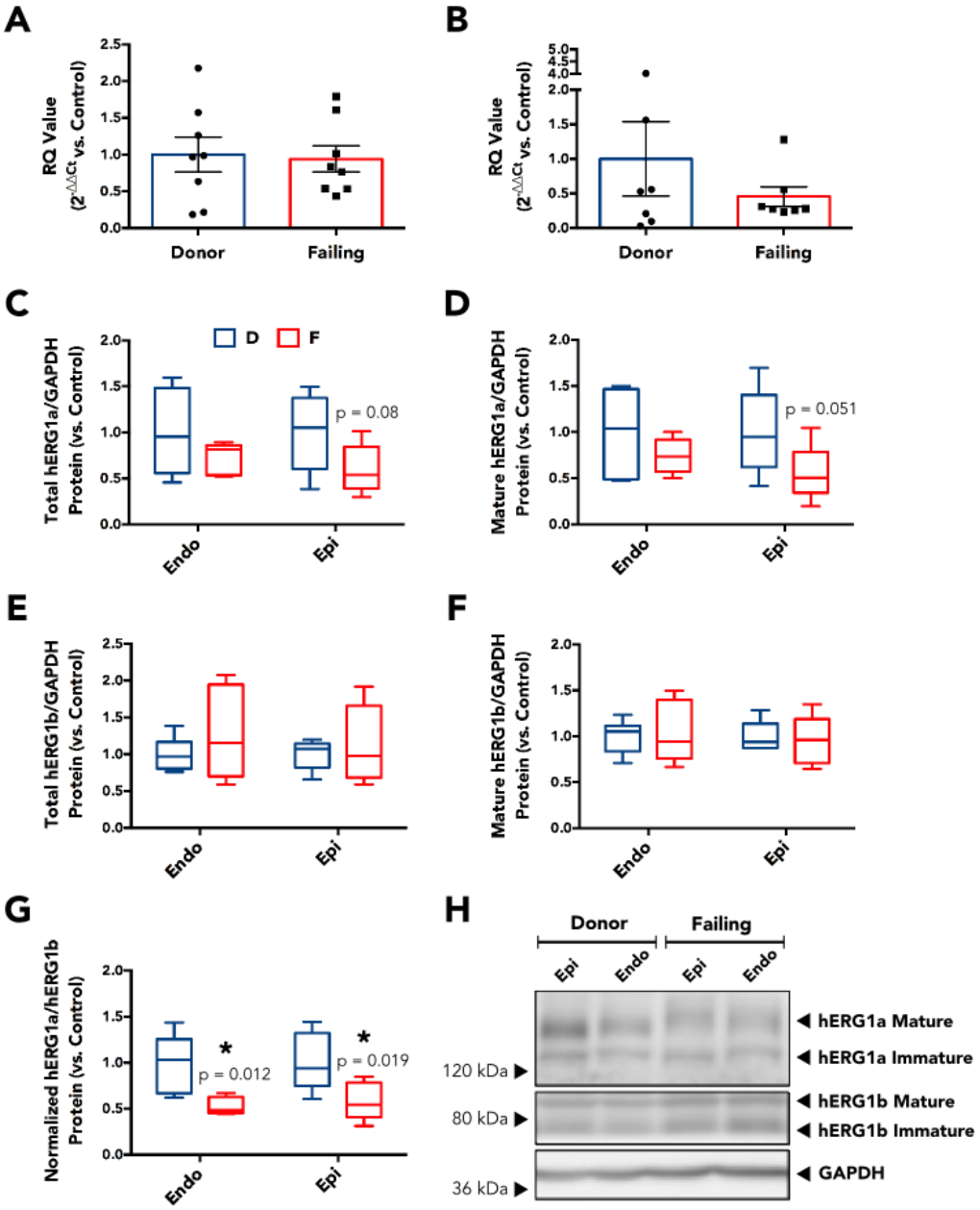

Computer simulation of myocyte I_{Kr} blockade. The effects of E-4031 were tested in isolated virtual nonfailing and failing endocardial myocytes. To simulate the effects of the drug, I_{Kr} conductance was reduced by 90% in nonfailing myocytes and by 90% or 70% in failing myocytes. Based on experimentally determined protein expression levels, with a stoichiometric shift from hERG1a to hERG1b, we assumed that the effect of the drug could be weaker in failing myocytes. Homotetrameric hERG1a channels have differential sensitivity to I_{Kr}-blocking drugs compared with hERG1a-hERG1b heteromeric channels, with hERG1a-hERG1b channels being less sensitive to E-4031.[24]

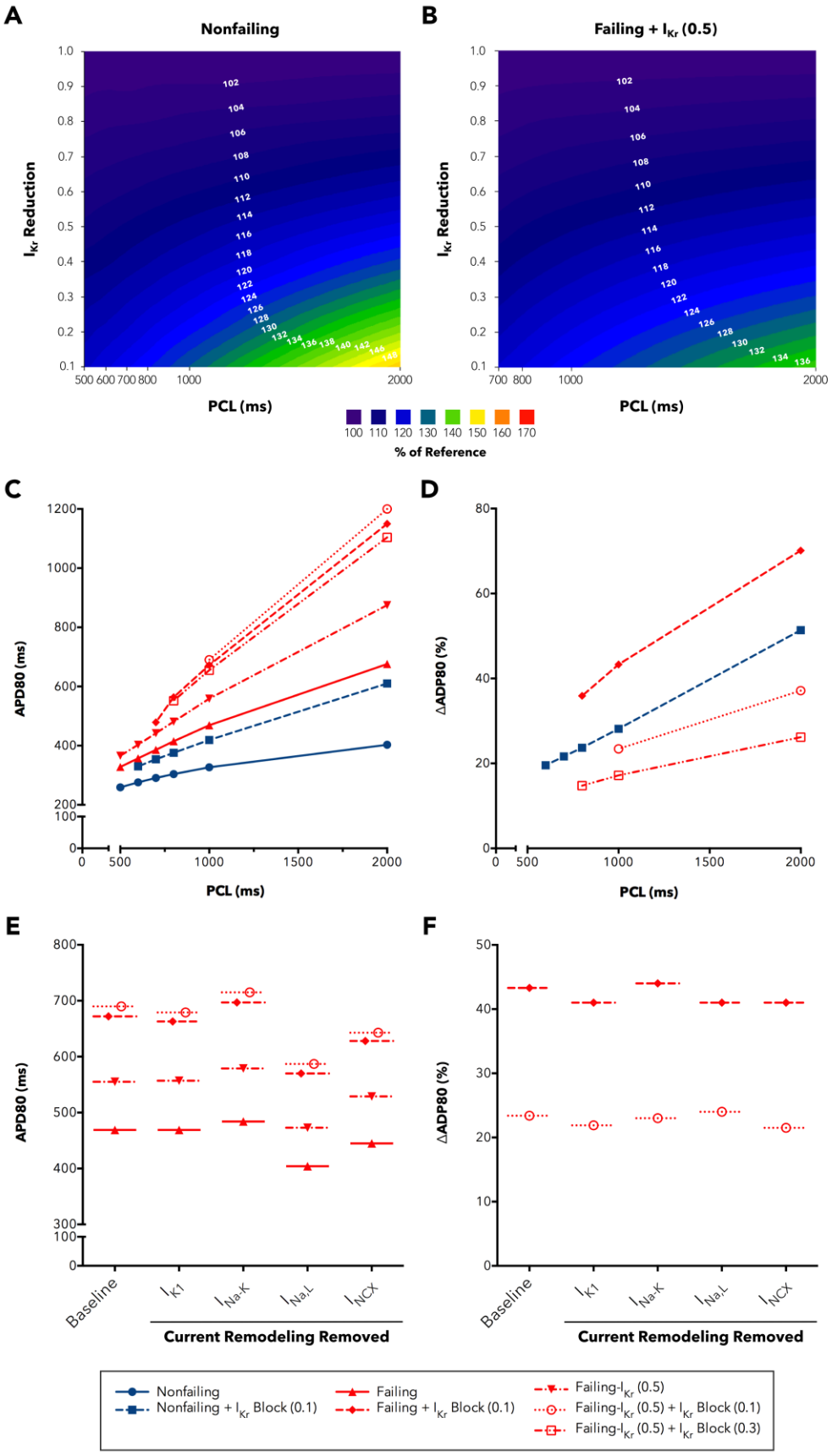
A
Nonfailing
B
Failing + I_{Kr} (0.5)
I_{Kr} Reduction
PCL (ms)
% of Reference
C
APD80 (ms)
PCL (ms)
D
ΔADP80 (%)
PCL (ms)
E
APD80 (ms)
Baseline
I_{K1}
$I_{Na\text{-}K}$
$I_{Na,L}$
I_{NCX}
Current Remodeling Removed
F
ΔADP80 (%)
Baseline
I_{K1}
$I_{Na\text{-}K}$
$I_{Na,L}$
I_{NCX}
Current Remodeling Removed
Nonfailing
Nonfailing + I_{Kr} Block (0.1)
Failing
Failing + I_{Kr} Block (0.1)
Failing-I_{Kr} (0.5)
Failing-I_{Kr} (0.5) + I_{Kr} Block (0.1)
Failing-I_{Kr} (0.5) + I_{Kr} Block (0.3)

247

The experimentally determined ΔAPD80 shows that the relative APD80 prolongation is greater in donor compared with failing myocytes. Thus, in order to reproduce experimental results, we carried out systematic cellular simulations for different PCLs with different degrees of block by E-4031 in nonfailing and failing myocytes, taking into account HF-induced I_{Kr} downregulation (Supplementary Figure S6). Figure 5A,B show color-coded maps of APD80 prolongation (relative to 100%), which is more pronounced in the case of nonfailing myocytes for different PCLs and different degrees of drug-induced block, than in the case of HF with 50% I_{Kr} downregulation. Figure 5C shows restitution curves for failing and nonfailing simulations with or without I_{Kr} drug block. Simulated APD80 values at low PCLs are not reported because of repolarization failure in the HF model. Figure 5D illustrates the corresponding drug-induced APD80 increase with respect to baseline in both failing and nonfailing conditions. Our simulations qualitatively reproduce experimental results provided that the model of HF includes I_{Kr} remodeling, i.e. a 50% downregulation in the cases illustrated in the two lower curves in Figure 5D. If I_{Kr} downregulation was not included in the HF model, APD80 increase with drug was much more pronounced than in normal myocytes. These results confirm our hypothesis that I_{Kr} is downregulated in HF, to a similar degree as determined by our experimental protein expression studies. To further examine the role that other currents play in AP prolongation due to I_{Kr} blockade, we repeated simulations at PCL = 1000 ms, while removing the HF remodeling of other important currents, including I_{K1}, $I_{Na\text{-}K}$, $I_{Na,L}$, and I_{NCX}. When these currents were not remodeled, APD80 values were altered before and after drug block (Figure 5E), thus impacting the ΔAPD80 for each condition (Figure 5F). However, with the removal of remodeling of any currents in the HF model, ΔAPD80 values were very similar to the HF model with just 50% I_{Kr} reduction. Also, in each case, the ΔAPD80 values are smaller than with the HF model without I_{Kr} downregulation, suggesting that I_{Kr} downregulation is key to replicating the experimental ΔAPD80 trend.

Multicellular simulation of I_{Kr} blockade. The results obtained in the multicellular strand simulations show a similar tendency: I_{Kr} remodeling was required in the HF model to obtain a lesser ΔAPD80 compared with nonfailing myocytes. Several cases of homogeneous and heterogeneous remodeling were considered. Figure 6A shows an illustrated schematic of our simulated 1D multicellular strand, with cones marking the endocardial and epicardial cells, which were used for measurements. Endocardial (upper panels) and epicardial (lower panels) APs are depicted for baseline and under the effects of E-4031 for nonfailing (Figure 6B,D; cells #50 and #150, respectively) and for failing (Figure 6C,E; cells #50 and #150, respectively). APD prolongation is greater in nonfailing myocytes than in failing myocytes.

Figure 6F shows nonfailing and failing restitution curves from endocardial and epicardial cells of the strand with simulated blockade by E-4031. Simulated APD80 values at low PCLs are not reported because of repolarization failure in the HF model. Note that E-4031 reduces I_{Kr} activity by 90% in nonfailing tissue and by 70% in failing tissue. ΔAPD80 caused by E-4031 is slightly more pronounced in the nonfailing tissue, as illustrated in Figure 6G. These results corroborate our experimental findings. Also, the ΔAPD80 values shown are greater in endocardium than in epicardium for both nonfailing and failing conditions. This effect is intrinsic to basic GPB model (see Figure 7B in Grandi et al.,[14]), where endocardial cells are more sensitive to I_{Kr} block than epicardial cells. In our HF model this effect is even more evident because I_{Kr} downregulation was more pronounced in epicardial cells than in endocardial cells, rendering the endocardium more responsive to I_{Kr} block.

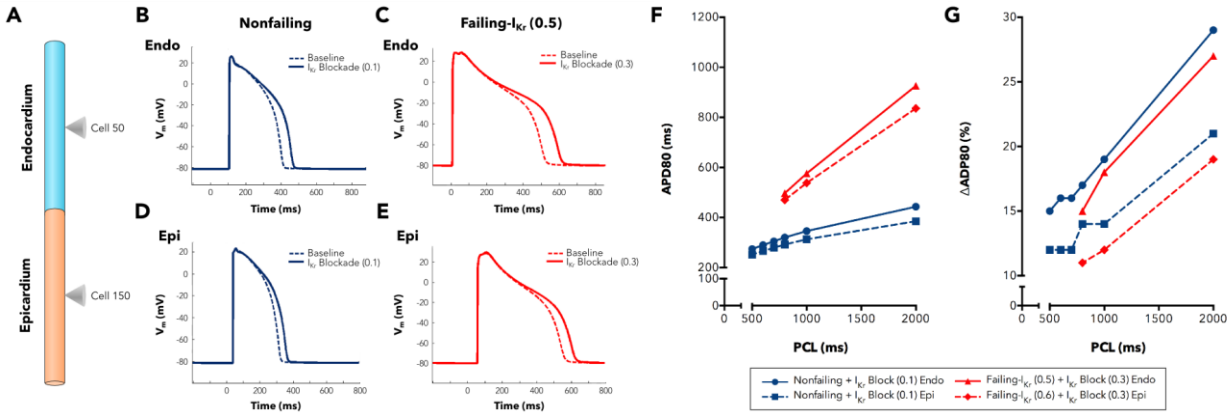

Discussion

Our results demonstrate functional downregulation of the E-4031 sensitive I_{Kr} current in the failing human heart, which may contribute to repolarization abnormalities and arrhythmogenesis in HF. While we observe a clear functional downregulation of I_{Kr} in the failing LV, these changes are not associated with gene expression changes for *hERG1a* or *hERG1b*. We posit that the lack of decreased *hERG1a* or *hERG1b* gene expression suggests transcriptional regulation of I_{Kr} is not a homeostatic mechanism in end-stage human HF, i.e. to preserve contractile force through AP prolongation, and this may contribute to the relatively small observed APD differences in failing compared with donor human hearts. Although gene expression is unaltered, we have demonstrated protein expression changes for hERG1a and hERG1b. Thus, we speculate that post-translational modifications and targeting of hERG channels may be the most critical factors governing I_{Kr} functional expression in failing human heart. Likewise, previous

studies have demonstrated that cell surface expression of Connexin43 and Cav1.2 are reduced in human HF due to impaired trafficking.[25, 26] Protein expression levels and post-translational effects on hERG1, resulting from general disruption in cardiomyocyte architecture and cellular trafficking in HF, are likely important regulators of I_{Kr} levels.

Alterations of hERG1 expression levels and stoichiometry underlie APD changes. Our results suggest that functional downregulation may be due to disruption of the cell surface protein expression (mature hERG1a), with contribution of a stoichiometric shift between hERG1a:hERG1b at the protein level. Larsen et al.[12] have shown greater levels of hERG1a than hERG1b in the human heart. Thus, decrements in hERG1a protein may have a greater influence on overall I_{Kr} levels. However, the shift in stoichiometry of hERG1a:hERG1b is due to a reduction in both mature and immature isoforms of hERG1a, combined with an increased trend in hERG1b.

Though the expression of the hERG1b isoform in the human heart has been somewhat controversial, with one report showing detection of the *hERG1b* transcript while another showed no hERG1b protein expression.[9, 12] However, the most critical demonstration of hERG1b function in the human heart was from Sale et al.[27], who identified the first long QT-linked mutation specifically within *hERG1b*. Our study is the first report of hERG1b in human cardiac tissue at both the transcript and protein levels; however, we acknowledge the difficulty in obtaining results for hERG1b protein expression from human cardiac tissue. Often, both hERG1a and hERG1b proteins were difficult to detect via Western blot. We primarily attribute this to the process for development and validation of antibodies, which are typically only tested against overexpressed hERG proteins in heterologous expression systems. Thus, when attempting to probe in human cardiac tissue, the low level of hERG1 protein relative to other cellular proteins makes detection challenging. We attempted to use several antibodies from various companies including Abcam, Alomone Labs, Cell Signaling Technology, Enzo Life Sciences, and Santa Cruz Biotechnology. Several of the antibodies yielded considerable non-specific binding; thus, we did not consider these results to be interpretable or accurate. Ultimately, we observed the sharpest results for hERG1a and hERG1b expression with the antibody from Alomone Labs, and confirmed specific hERG1b expression with the hERG1b antibody from Enzo Life Sciences (Supplementary Figure S4).

Optical imaging of LV wedge preparations versus an isolated cell approach. In many experimental systems, whole-cell voltage clamp is the gold standard for measuring functional channel cell surface

expression,[28-30] and I_{Kr} has been successfully recorded in isolated cardiomyocytes from undiseased human hearts.[31, 32] However, we have not used cell isolation and patch-clamp methods for several reasons. Delayed-rectifier current levels are small in cardiomyocytes, because these channels operate on the portion of the AP where membrane resistance is high; thus minor changes in K^+ current flux lead to large changes in membrane potential.[33] The amplitude of representative I_{Kr} tail current in human cardiac myocytes was shown to be ~50 pA, which contrasts with other human cardiac ion currents that are hundreds of pAs to nAs in amplitude, such as I_{Na} or I_{K1}.[31, 32] In addition, the cell isolation process has been shown to specifically disrupt the membrane expression of delayed rectifier K^+ channels. This effect should be particularly pronounced for the digestion of human myocardium, which requires harsh digestion conditions due to the high level of fibrotic tissue, especially in failing hearts. Presumably, due to the combination of these effects, Beuckelmann and colleagues were unable to analyze delayed-rectifier K^+ currents in isolated cells from donor or failing hearts. In this study, delayed-rectifier currents were either small or non-existent, which prohibited comparison between groups.[2, 34] Thus, due to the relatively small amplitude of I_{Kr} in even nondiseased human cardiomyocytes, and the variability in current amplitude demonstrated by Beuckelmann et al.[2], we concluded that differences I_{Kr} between donor and failing heart populations would be difficult to reliably detect without prohibitively large sample numbers.

Instead, we have relied on changes in APD following I_{Kr} blockade to serve as an indicator for functional expression. Although the E-4031 blocker utilized is highly specific for I_{Kr}, we recognize that our approach does not completely isolate the effects of this single current on ΔAPD. Cardiac APs are the composite of dynamic responses from many currents, and, thus, ΔAPDs from blocking I_{Kr} cannot be solely attributed to the density of I_{Kr}. Simulation studies using multivariate correlation analysis of ΔAPD from I_{Kr} blockade show that I_{Kr} conductance is the most strongly (positively) associated model parameter, but that many other parameters are also correlated with ΔAPD.[35, 36] These other parameters include conductances and kinetics of many ion channels, such as I_{K1}, I_{Ks} and $I_{Na,L}$, which may be positively or negatively associated with ΔAPD from I_{Kr} blockade. However, the added power of our approach is the ability to obtain AP recordings from many cells within tissue, and from different transmural regions; thus, providing additional information that more closely approximates the behavior in the intact human heart. We also consider the magnitude of the experimental effect to be quite profound, with ~70% increase in APD80 after I_{Kr} blockade in donor compared with only ~30% increase in failing hearts. This large experimental difference supports that a reduction in I_{Kr} conductance is a major contributing factor to the differential response to I_{Kr} blockade in donor versus failing hearts.

Optical mapping of LV wedge preparations has also enabled us to confirm other aspects of EP remodeling in the failing human heart that have formerly been reported by our group. We have previously found transmural gradients in APD to be reduced in failure[3, 4, 23, 37], which we also observed in this study. In two preparations, we also identified some tissue areas that would have been labeled as M cell islands by the definition used in Glukhov et al.[23]

Reduced ΔAPD80s in failing and the Law of Initial Values. Our results also indicate that the reduced percent increase in APD following I_{Kr} blockade is not due to the Law of Initial Value (LIV),[38, 39] which would assert that the reduced ΔAPD80s in failing are due to higher baseline values. Although, the underlying mechanism for a LIV effect is unknown, the prolonged APs in failing would be closer to a theoretical APD upper limit. Following I_{Kr} blockade, not only was ΔAPD80 greater for donor hearts, but also the absolute duration of APs was greater compared with failing hearts, further suggesting functional I_{Kr} downregulation in failure.

I_{Kr} downregulation in HF computational models. Our computer simulations qualitatively reproduced the experimental I_{Kr} downregulation. As stated above, there was previously no experimental evidence of I_{Kr} downregulation in the failing human heart, and results of delayed rectifier current expression from animal models of HF are strikingly inconsistent. Tsuji and colleagues found that, in the rabbit pacing-induced HF model, both E-4031-sensitive and -resistant components were significantly smaller than those in control hearts.[40] In addition, decreased activity of the delayed rectifier current was observed in ventricular myocytes obtained from cats with hypertrophy.[41] In contrast, studies of isolated myocytes from the pressure overload guinea pig or spontaneously hypertensive rat models documented no change in I_{Kr}. Likewise, I_{Kr} also remained unchanged in canine models of HF.[42] [43, 44] Thus, in previous simulation studies, I_{Kr} downregulation has not been incorporated in computational HF models, regardless of species.[45-47] Only Walmsley et al.[17] considered I_{Kr} downregulation in their HF computer model on the basis of our group's previous experimental findings on gene expression changes in HF.[11] Our simulations illustrate for the first time that I_{Kr} downregulation must be incorporated in HF remodeling to obtain a smaller E-4031-induced APD80 prolongation than in nonfailing conditions, as obtained experimentally in the present study.

Another aspect shown in our simulations and in previous computational studies, is that I_{Kr} block-induced APD prolongation does not only depend on the amount of I_{Kr} but also on the amount of other currents conductance (see Figure 6F). Similarly, a computational study based on Luo and Rudy dynamic

model (Luo and Rudy 1994) by Saiz et al. (Saiz et al., 2011) obtained different APD prolongations with the same dose of dofetilide in endocardial, epicardial, and M cells, which present differences in I_{Ks} conductance. Also Brennan et al. (Brennan et al., 2009) used TNNP (Ten Tusscher 2006) model and obtained different APD prolongations with sotalol in the different ventricular cells having different Ito and I_{Ks} conductances. Finally, Mirams et al. (Mirams et al., 2011) highlighted the importance of including three (instead of I_{Kr} only) ion-channel effects to the predictive classification of drugs into the risk categories established by Redfern (Redfern et al., 2003). They suggested that AP modeling of multiple ion-channel effects may improve early identification of clinical risk and that torsadogenic effects of hERG block can be eliminated by inhibiting additional channels. Although it is important to take into account that I_{Kr} block-induced APD prolongation is affected by other ion currents, we can conclude from our simulations that I_{Kr} downregulation leads to lower I_{Kr} block-induced APD prolongations than in the absence of I_{Kr} downregulation. Indeed, as demonstrated the simulation studies by Britton et al. (Britton et al., 2013) and Sarkar et al. (Sarkar et al., 2011), I_{Kr} conductance is the ionic parameter which affects the most APD prolongation after drug induced I_{Kr} block, much more than other ion channel conductances. Also the sensitivity analyses performed by O'hara et al. (O'Hara et al., 2011) and Walmsley et al. (Walmsley et al., 2013) showed that I_{Kr} downregulation had a bigger effect on APD prolongation than remodeling of other ion currents in control conditions. This held for failing myocytes (Walmsley et al., 2013).

Limitations

Our protocol required the use of blebbistatin in order to acquire APs free of motion artifact. Blebbistatin has been previously shown not to affect electrophysiology in multiple species, including humans.[48] In addition, because we work with human tissue, we take hearts for study as they become available; thus, we have a varied and uncontrolled population in comparison to animal models research. There are other important factors upon which we are unable to perfectly match our donor and failing heart groups, including age and gender.

Our computer myocyte model for HF, based on changes in the ion channel parameters, has the inherited limitations described in Trenor et al.[15] Mainly, data from a large number of experimental studies were taken into account, thus resulting in a high variability not only in the ionic remodeling but also in the stage and etiology of HF and its phenotype. This computer model was validated against experimental data of AP and Ca^{2+} transient measurements in human failing hearts. APD prolongation in

HF was 43% using the baseline HF model; this value is within the experimental range[45, 49]. In the present study, when I_{Kr} downregulation was also included in the HF model, APD prolongation was more pronounced (70%). The experimental studies by Beuckelman et al.[2, 50] also reported a pronounced APD increase (60-67%) in HF.[2, 50] Given the existent experimental variability in HF measurements, various combinations of ion current remodeling values would yield a HF phenotype within experimental ranges. In this way, the simulation study by Walmsley et al.[17] considers a polulation of HF models to account for the experimental variability.

It is also to be noted that the baseline GPB model has an APD80 within experimental ranges taken from other studies, but significantly shorter than the experimental measurements shown in the present work. The absolute APD80 values simulated with our HF model also present significant differences with our experimental measurements. The comparison between experiments and simulations should not be strictly quantitative but rather qualitative, given the high experimental variability. We would like to highlight again that these simulations are a proof of concept rather than a strict reproduction of the experimental quantitative results.

In spite of its inherent limitations, the HF model utilized in the present study provides valid proof-of-concept and reinforcement of our experimental findings.

Figure Legends

Figure 1. Experimental methodology. A. Posterolateral image of a human heart. Black dashed box outlines marginal artery territory for wedge preparation, and black arrowheads indicate two descending marginal arteries. **B.** Representative wedge preparation image with paired optical (blue) and microelectrode (red) recordings. Wedge transmural regions separated by dashed lines, and black and red arrows highlight pacing and microelectrodes, respectively. **C.** Timeline of the experimental protocol. A=aorta; Epi=epicardium; Endo=endocardium; LA=left atrium; LV=left ventricle; RA=right atrium; RV=right ventricle.

Figure 2. APD80 restitution before and after I_{Kr} blockade. Restitution curves for the pacing cycle length (PCL) versus APD80 for **A.** donor (n=7) and **D.** failing (n=4) hearts at baseline, demonstrating greater transmural APD80 dispersion for donor hearts and higher APD80s for failing hearts. APD80 restitution

curves for **B.** donor and **E.** failing hearts after I_{Kr} blockade with E-4031. In contrast to the baseline conditions, absolute APD80 values are now greater in donor compared with failing hearts. APD80 gradients ($APD80_{Endo}$ – $APD80_{Epi}$) at several PCLs for **C.** baseline and **F.** E-4031 conditions. Data are expressed as mean ± SEM.

Figure 3. ΔAPD80 values with I_{Kr} blockade. A-B. Representative APD80 maps, optical recording traces, and pseudo-ECGs for donor and failing hearts. Gaussian distribution curves calculated from means and pooled standard deviations of APD80 values for **C.** donor and **D.** failing hearts. **E.** Average APD80 values for donor (n=7) and failing (n=4) hearts under control and E-4031 conditions recorded at 1000 ms pacing cycle length (PCL). **F.** ΔAPD80s, expressed as a % of control for 1000 ms PCLs. Data are expressed as mean ± SEM.

Figure 4. hERG1 gene and protein expression levels. Graphs with individual data points showing *hERG1a* **A.** and *hERG1b* **B.** gene expression is not different between donor (n=8) and failing (n=8) human hearts. Box and whisker plots of total hERG1a **C.** and mature hERG1a **D.** relative to GAPDH show that failing (n=5) compared with donor (n=6) heart hERG1a levels trend toward reduction. Graphs demonstrating total **E.** and mature **F.** hERG1b protein expression levels are unchanged. **G.** Graph showing significantly decreased hERG1a:hERG1b protein in the failing epicardium. **H.** Representative Western blot image. Bar graphs show data expressed as mean ± SEM. Boxes show median, 25% percentile, and 75% percentile, and whiskers indicate the minimum and maximum of the distribution.

Figure 5. Cellular simulation results. A,B. Color-coded maps of APD increase (relative to 100%) in nonfailing myocytes and failing myocytes with I_{Kr} blockade. The results are shown for different pacing cycle lengths (PCLs, x-axis) and for different degrees of drug block (y-axis). The model of HF considers I_{Kr} downregulation by 0.5. **C.** APD80 restitution curves for nonfailing, failing, and failing with I_{Kr} downregulation myocytes with and without I_{Kr} blockade. **D**.ΔAPD80s with I_{Kr} blockade (90% or 70%), expressed as a % of control in a nonfailing cell and in failing cells with or without I_{Kr} downregulation. **E**. APD80 values plus and minus I_{Kr} blockade for failing cells with and without I_{Kr} downregulation at PCL = 1000 ms. Baseline APD80 values and values after removal of HF remodeling for I_{K1}, $I_{Na\text{-}K}$, $I_{Na,L}$, and I_{NCX} are displayed. **F**. ΔAPD80s after I_{Kr} blockade for failing myocytes with and without I_{Kr} downregulation are shown for baseline conditions and after removing remodeling for I_{K1}, $I_{Na\text{-}K}$, $I_{Na,L}$, and I_{NCX} in the HF simulations.

Figure 6. Multicellular strand simulations. A. Illustrated schematic of the multicellular strand for simulations, including endocardial and epicardial cells and cones marking the cells used for measurement. **B.** Nonfailing and **C.** failing endocardial myocyte APs before and after I_{Kr} blockade with E-4031 (cell #50). **D**. Nonfailing and **E.** failing epicardial myocytes APs before and after I_{Kr} blockade with E-4031 (cell #150). **F.** APD80 restitution curves of cells #50 (endocardium) and #150 (epicardium) for nonfailing and failing conditions. Drug blockade was 90% in nonfailing cells and 70% in failing cells. **G**. ΔAPD80s expressed as a % of control in cells #50 (endocaridum) and #150 (epicardium) for nonfailing and failing conditions under I_{Kr} blockade with E-4031. Drug blockade was 90% in nonfailing cells and 70% in failing cells.

Table 1. Demographic characteristics of donor and failing hearts used for optical imaging analysis. CVA=cerebrovascular accident; D=donor; F=failing; ICH=intracerebral hemorrhage; ICM=ischemic cardiomyopathy; MVA=motor vehicle accident; NICM=nonischemic cardiomyopathy.

D/F	Age	Gender	Diagnosis/ Cause of Death
D	17	F	MVA
D	37	F	CVA
D	39	M	ICH
D	52	M	MVA
D	58	M	CVA
D	60	M	CVA
D	65	M	CVA
F	44	F	NICM
F	55	M	ICM
F	57	M	ICM
F	59	F	NICM

Table 2. Detailed ionic current modifications to GPB model for failing cardiac myoctes. These model manipulations were previously published in Trenor et al.**[15]**

Parameter modified	% of change respect original GPB model[14]	References
I_{NaL}	↑200	Valdivia et al. 2005.[7], Maltsev et al. 2007.[51]
τ_{NaL}	↑200	Maltsev et al. 2007.[51],
I_{to}	↓60	Beuckelmann et al. 1993.[2], Wettwer et al. 1994.[52], Nabauer et al. 1996.[53]
I_{K1}	↓32	Beuckelmann et al. 1993.[2], Tomaselli and Marban. 1999.[54], Li et al. 2004.[49]
I_{NaK}	↓10	Bundgaard et al. 1996.[55], Tomaselli and Marban. 1999.[54], Tomaselli and Zipes. 2004.[1]
I_{Nab}	=0	Priebe and Beuckelmann. 1998.[45]
I_{Cab}	↑153	Priebe and Beuckelmann. 1998.[45]
I_{NCX}	↑175	Priebe and Beuckelmann. 1998.[45]
I_{SERCA}	↓50	Hasenfuss et al. 1994.[56], Schwinger et al. 1995.[57], Piacentino et al. 2003.[20]
I_{leak}	↑500	Bers et al. 2006.[58]
EC_{50SR}	↓11	Bers et al. 2006.[58], Antoons et al. 2007.[59], Curran et al. 2010.[60]

Disclosure and conflicts of interest

None

Acknowledgements

We thank the Translational Cardiovascular Biobank & Repository (TCBR) at Washington University for provision of donor/patient records. The TCBR is supported by the NIH/CTSA (UL1 TR000448), Children's Discovery Institute, and Richard J. Wilkinson Trust. We also thank the laboratory of Dr. Sakiyama-Elbert for the use of the StepOnePlus equipment. We appreciate the critical feedback on the manuscript by Dr. Jeanne Nerbonne. This work has been supported by the National Heart, Lung & Blood Institute (NHLBI, R01 HL114395). K. Holzem has been supported by the American Heart Association (12PRE12050315) and the NHLBI (F30 HL114310).

References

[1] Tomaselli GF, Zipes DP. What causes sudden death in heart failure? Circ Res. 2004;95:754-63.
[2] Beuckelmann DJ, Nabauer M, Erdmann E. Alterations of K+ currents in isolated human ventricular myocytes from patients with terminal heart failure. Circ Res. 1993;73:379-85.
[3] Glukhov AV, Fedorov VV, Kalish PW, Ravikumar VK, Lou Q, Janks D, et al. Conduction Remodeling in Human End-Stage Non-Ischemic Left Ventricular Cardiomyopathy. Circulation. 2012.
[4] Lou Q, Fedorov VV, Glukhov AV, Moazami N, Fast VG, Efimov IR. Transmural heterogeneity and remodeling of ventricular excitation-contraction coupling in human heart failure. Circulation. 2011;123:1881-90.
[5] Akar FG, Rosenbaum DS. Transmural electrophysiological heterogeneities underlying arrhythmogenesis in heart failure. Circ Res. 2003;93:638-45.
[6] Maltsev VA, Sabbah HN, Higgins RS, Silverman N, Lesch M, Undrovinas AI. Novel, ultraslow inactivating sodium current in human ventricular cardiomyocytes. Circulation. 1998;98:2545-52.
[7] Valdivia CR, Chu WW, Pu J, Foell JD, Haworth RA, Wolff MR, et al. Increased late sodium current in myocytes from a canine heart failure model and from failing human heart. J Mol Cell Cardiol. 2005;38:475-83.
[8] Undrovinas AI, Maltsev VA, Kyle JW, Silverman N, Sabbah HN. Gating of the late Na+ channel in normal and failing human myocardium. J Mol Cell Cardiol. 2002;34:1477-89.
[9] Pond AL, Nerbonne JM. ERG proteins and functional cardiac I(Kr) channels in rat, mouse, and human heart. Trends Cardiovasc Med. 2001;11:286-94.

[10] Laughner JI, Ng FS, Sulkin MS, Arthur RM, Efimov IR. Processing and analysis of cardiac optical mapping data obtained with potentiometric dyes. American Journal of Physiology-Heart and Circulatory Physiology. 2012;303:H753-H65.
[11] Ambrosi CM, Yamada KA, Nerbonne JM, Efimov IR. Gender differences in electrophysiological gene expression in failing and non-failing human hearts. PLoS One. 2013;8:e54635.
[12] Larsen AP, Olesen SP, Grunnet M, Jespersen T. Characterization of hERG1a and hERG1b potassium channels-a possible role for hERG1b in the I (Kr) current. Pflugers Arch. 2008;456:1137-48.
[13] Livak KJ, Schmittgen TD. Analysis of relative gene expression data using real-time quantitative PCR and the 2-[Delta][Delta] CT method. Methods. 2001;25:402-8.
[14] Grandi E, Pasqualini FS, Bers DM. A novel computational model of the human ventricular action potential and Ca transient. J Mol Cell Cardiol. 2010;48:112-21.
[15] Trenor B, Cardona K, Gomez JF, Rajamani S, Ferrero Jr JM, Belardinelli L, et al. Simulation and mechanistic investigation of the arrhythmogenic role of the late sodium current in human heart failure. PloS one. 2012;7:e32659.
[16] Soltysinska E, Olesen S-P, Christ T, Wettwer E, Varró A, Grunnet M, et al. Transmural expression of ion channels and transporters in human nondiseased and end-stage failing hearts. Pflügers Archiv-European Journal of Physiology. 2009;459:11-23.
[17] Walmsley J, Rodriguez JF, Mirams GR, Burrage K, Efimov IR, Rodriguez B. mRNA expression levels in failing human hearts predict cellular electrophysiological remodeling: A population-based simulation study. PLoS One. 2013;8:e56359.
[18] Xiong W, Tian Y, DiSilvestre D, Tomaselli GF. Transmural heterogeneity of Na+–Ca2+ exchange evidence for differential expression in normal and failing hearts. Circ Res. 2005;97:207-9.
[19] Gomez JF, Cardona K, Romero L, Ferrero Jr JM, Trenor B. Electrophysiological and Structural Remodeling in Heart Failure Modulate Arrhythmogenesis. 1D Simulation Study. PloS one. 2014;9:e106602.
[20] Piacentino V, 3rd, Weber CR, Chen X, Weisser-Thomas J, Margulies KB, Bers DM, et al. Cellular basis of abnormal calcium transients of failing human ventricular myocytes. Circ Res. 2003;92:651-8.
[21] Reinecke H, Studer R, Vetter R, Holtz J, Drexler H. Cardiac Na+/Ca2+ exchange activity in patients with end-stage heart failure. Cardiovasc Res. 1996;31:48-54.
[22] Iyer V, Heller V, Armoundas AA. Altered spatial calcium regulation enhances electrical heterogeneity in the failing canine left ventricle: implications for electrical instability. J Appl Physiol. 2012;112:944-55.
[23] Glukhov AV, Fedorov VV, Lou Q, Ravikumar VK, Kalish PW, Schuessler RB, et al. Transmural dispersion of repolarization in failing and nonfailing human ventricle. Circ Res. 2010;106:981-91.
[24] Abi- Gerges N, Holkham H, Jones E, Pollard C, Valentin JP, Robertson G. hERG subunit composition determines differential drug sensitivity. Br J Pharmacol. 2011;164:419-32.
[25] Smyth JW, Hong TT, Gao D, Vogan JM, Jensen BC, Fong TS, et al. Limited forward trafficking of connexin 43 reduces cell-cell coupling in stressed human and mouse myocardium. The Journal of clinical investigation. 2010;120:266-79.

[26] Hong TT, Smyth JW, Chu KY, Vogan JM, Fong TS, Jensen BC, et al. BIN1 is reduced and Cav1.2 trafficking is impaired in human failing cardiomyocytes. Heart rhythm : the official journal of the Heart Rhythm Society. 2012;9:812-20.
[27] Sale H, Wang J, O'Hara TJ, Tester DJ, Phartiyal P, He JQ, et al. Physiological properties of hERG 1a/1b heteromeric currents and a hERG 1b-specific mutation associated with Long-QT syndrome. Circ Res. 2008;103:e81-95.
[28] Baroudi G, Pouliot V, Denjoy I, Guicheney P, Shrier A, Chahine M. Novel mechanism for Brugada syndrome: defective surface localization of an SCN5A mutant (R1432G). Circ Res. 2001;88:E78-83.
[29] Furutani M, Trudeau MC, Hagiwara N, Seki A, Gong Q, Zhou Z, et al. Novel mechanism associated with an inherited cardiac arrhythmia: defective protein trafficking by the mutant HERG (G601S) potassium channel. Circulation. 1999;99:2290-4.
[30] Krumerman A, Gao X, Bian JS, Melman YF, Kagan A, McDonald TV. An LQT mutant minK alters KvLQT1 trafficking. American journal of physiology Cell physiology. 2004;286:C1453-63.
[31] Iost N, Virag L, Opincariu M, Szecsi J, Varro A, Papp JG. Delayed rectifier potassium current in undiseased human ventricular myocytes. Cardiovasc Res. 1998;40:508-15.
[32] Magyar J, Iost N, Körtvély Á, Banyasz T, Virag L, Szigligeti P, et al. Effects of endothelin-1 on calcium and potassium currents in undiseased human ventricular myocytes. Pflügers Archiv. 2000;441:144-9.
[33] Nerbonne JM, Kass RS. Molecular physiology of cardiac repolarization. Physiol Rev. 2005;85:1205-53.
[34] Veldkamp MW, van Ginneken AC, Opthof T, Bouman LN. Delayed rectifier channels in human ventricular myocytes. Circulation. 1995;92:3497-504.
[35] Britton OJ, Bueno-Orovio A, Van Ammel K, Lu HR, Towart R, Gallacher DJ, et al. Experimentally calibrated population of models predicts and explains intersubject variability in cardiac cellular electrophysiology. Proc Natl Acad Sci U S A. 2013;110:E2098-E105.
[36] Sarkar AX, Sobie EA. Quantification of repolarization reserve to understand interpatient variability in the response to proarrhythmic drugs: A computational analysis. Heart Rhythm. 2011;8:1749-55.
[37] Ng FS, Holzem KM, Koppel AC, Janks D, Gordon F, Wit AL, et al. Adverse Remodeling of the Electrophysiological Response to Ischemia–Reperfusion in Human Heart Failure Is Associated With Remodeling of Metabolic Gene Expression. Circulation: Arrhythmia and Electrophysiology. 2014;7:875-82.
[38] Hord DJ, Johnson LC, Lubin A. Differential effect of the law of initial value (LIV) on autonomic variables. Psychophysiology. 1964;1:79-87.
[39] Tu YK, Gilthorpe MS. Revisiting the relation between change and initial value: a review and evaluation. Stat Med. 2007;26:443-57.
[40] Tsuji Y, Opthof T, Kamiya K, Yasui K, Liu W, Lu Z, et al. Pacing-induced heart failure causes a reduction of delayed rectifier potassium currents along with decreases in calcium and transient outward currents in rabbit ventricle. Cardiovasc Res. 2000;48:300-9.
[41] Furukawa T, Bassett A, Furukawa N, Kimura S, Myerburg R. The ionic mechanism of reperfusion-induced early afterdepolarizations in feline left ventricular hypertrophy. J Clin Invest. 1993;91:1521.

[42] Li GR, Lau CP, Ducharme A, Tardif JC, Nattel S. Transmural action potential and ionic current remodeling in ventricles of failing canine hearts. American journal of physiology Heart and circulatory physiology. 2002;283:H1031-41.
[43] Brooksby P, Levi AJ, Jones JV. Investigation of the mechanisms underlying the increased contraction of hypertrophied ventricular myocytes isolated from the spontaneously hypertensive rat. Cardiovasc Res. 1993;27:1268-77.
[44] Ahmmed GU, Dong PH, Song G, Ball NA, Xu Y, Walsh RA, et al. Changes in Ca2+ cycling proteins underlie cardiac action potential prolongation in a pressure-overloaded guinea pig model with cardiac hypertrophy and failure. Circ Res. 2000;86:558-70.
[45] Priebe L, Beuckelmann DJ. Simulation study of cellular electric properties in heart failure. Circ Res. 1998;82:1206-23.
[46] Moreno JD, Zhu ZI, Yang P-C, Bankston JR, Jeng M-T, Kang C, et al. A computational model to predict the effects of class I anti-arrhythmic drugs on ventricular rhythms. Science translational medicine. 2011;3:98ra83-98ra83.
[47] Zhang Y, Shou G, Xia L. Simulation study of transmural cellular electrical properties in failed human heart. Engineering in Medicine and Biology Society, 2005 IEEE-EMBS 2005 27th Annual International Conference of the: IEEE; 2006. p. 337-40.
[48] Fedorov VV, Lozinsky IT, Sosunov EA, Anyukhovsky EP, Rosen MR, Balke CW, et al. Application of blebbistatin as an excitation-contraction uncoupler for electrophysiologic study of rat and rabbit hearts. Heart rhythm : the official journal of the Heart Rhythm Society. 2007;4:619-26.
[49] Li GR, Lau CP, Leung TK, Nattel S. Ionic current abnormalities associated with prolonged action potentials in cardiomyocytes from diseased human right ventricles. Heart Rhythm. 2004;1:460-8.
[50] Beuckelmann DJ, Erdmann E. Ca(2+)-currents and intracellular [Ca2+]i-transients in single ventricular myocytes isolated from terminally failing human myocardium. Basic Res Cardiol. 1992;87 Suppl 1:235-43.
[51] Maltsev VA, Silverman N, Sabbah HN, Undrovinas AI. Chronic heart failure slows late sodium current in human and canine ventricular myocytes: Implications for repolarization variability. European Journal of Heart Failure. 2007;9:219-27.
[52] Wettwer E, Amos GJ, Posival H, Ravens U. Transient outward current in human ventricular myocytes of subepicardial and subendocardial origin. Circ Res. 1994;75:473-82.
[53] Nabauer M, Beuckelmann DJ, Uberfuhr P, Steinbeck G. Regional differences in current density and rate-dependent properties of the transient outward current in subepicardial and subendocardial myocytes of human left ventricle. Circulation. 1996;93:168-77.
[54] Tomaselli GF, Marban E. Electrophysiological remodeling in hypertrophy and heart failure. Cardiovasc Res. 1999;42:270-83.
[55] Bundgaard H, Kjeldsen K. Human myocardial Na,K-ATPase concentration in heart failure. Mol Cell Biochem. 1996;163-164:277-83.
[56] Hasenfuss G, Reinecke H, Studer R, Meyer M, Pieske B, Holtz J, et al. Relation between myocardial function and expression of sarcoplasmic reticulum Ca (2+)-ATPase in failing and nonfailing human myocardium. Circ Res. 1994;75:434-42.
[57] Schwinger RH, Böhm M, Schmidt U, Karczewski P, Bavendiek U, Flesch M, et al. Unchanged protein levels of SERCA II and phospholamban but reduced Ca2+ uptake and Ca2+-ATPase activity of cardiac sarcoplasmic reticulum from dilated cardiomyopathy patients compared with patients with nonfailing hearts. Circulation. 1995;92:3220-8.

[58] Bers DM, Despa S, Bossuyt J. Regulation of Ca2+ and Na+ in normal and failing cardiac myocytes. In: Sideman S, Beyar R, Landesberg A, editors. Interactive and Integrative Cardiology2006. p. 165-77.
[59] Antoons G, Oros A, Bito V, Sipido KR, Vos MA. Cellular basis for triggered ventricular arrhythmias that occur in the setting of compensated hypertrophy and heart failure: considerations for diagnosis and treatment. J Electrocardiol. 2007;40:S8-S14.
[60] Curran J, Brown KH, Santiago DJ, Pogwizd S, Bers DM, Shannon TR. Spontaneous Ca waves in ventricular myocytes from failing hearts depend on Ca2+-calmodulin-dependent protein kinase II. J Mol Cell Cardiol. 2010;49:25-32.